MicroRNA detection on microsensor arrays by SPR imaging measurements with enzymatic signal enhancement

Hiroshi Aoki[1,2*], Robert M. Corn[2], Brandon Matthews[2]

[1] Environmental Management Research Institute, National Institute of Advanced Industrial Science and Technology (AIST), 16-1 Onogawa, Tsukuba, Ibaraki 305-8569, Japan

[2] Department of Chemistry, University of California, Irvine, Irvine, CA 92697, USA

[*] To whom correspondence should be addressed.

phone, +81-29-861-8050; e-mail, aoki-h@aist.go.jp

Abstract

We investigated sequence-specific and simultaneous microRNA (miRNA) detections by surface plasmon resonance (SPR) imaging measurements on SPR chips possessing an Au spot array modified with probe DNAs based on a miRNA-detection-selective SPR signal amplification method. MiRNAs were detected with the detection limit of the attomole level by SPR imaging measurements for different miRNA concentrations on a single chip. SPR signals were enhanced based on a combination process of sequence-specific hybridization of the miRNA to the probe DNAs, extension reaction of polyadenine (poly(A)) tails by poly(A) polymerase, binding of a ternary complex of T_{30}-biotin/horseradish peroxidase (HRP)-biotin/streptavidin to the poly(A) tails, and the oxidation reaction of tetramethylbenzidine (TMB) on the HRP by providing a blue precipitate on the surface. This process sequence-specifically and dramatically amplified the SPR signals. This is a simple, cost-effective, and feasible signal amplification method based on the organic compound TMB instead of metal nanoparticles.

Keywords: Surface plasmon resonance imaging; SPRI; RNA; detection; enzymatic amplification

1. Introduction

Oligonucleotide detection-based tests, including safety screening for environmental chemical toxicity and healthcare management, are increasingly being adopted in the fields of environmental and biomedical evaluation.(Alexander-Dann et al. 2018; Huang 2013; Huang et al. 2011; Wagner and Plewa 2017) This has prompted a great deal of research into tests based on differences in DNA sequences between wild types and mismatch types or on differences in RNA expression as a transcriptome. Considerable efforts have been focused on RNA expression to reveal the difference between wellness and sickness or states with and without stress. They demonstrate that RNA expression can be used to evaluate biological responses to external stimuli.(Fukushima et al. 2014; Igarashi et al. 2015; Rakszewska et al. 2016)

Micro RNAs (miRNAs), i.e., short non-coding RNAs with a length of 20–25 bases, regulate the translation or degradation of messenger RNAs (mRNAs), i.e., coding RNAs with genetic information.(Siomi and Siomi 2010) MiRNAs are increasingly being studied by numerous researchers, including the potential application of miRNA-based tests to the evaluation of stresses caused by environmental chemicals and to the diagnosis of lifestyle-related diseases or cancers.(Angelini and Emanueli 2015; Kreth et al. 2018; Leung and Sharp 2010; Mendell and Olson 2012; Min and Chan 2015; Olejniczak et al. 2018) MiRNAs as biomarker for cancers have also been elaborated by many researchers in the past decade.(Bonci et al. 2016; Hayes et al. 2014; Hofbauer et al. 2018; Jansson and Lund 2012; Mihelich et al. 2015) Since miRNA is found in blood samples, which can be drawn routinely and minimally invasively, the utilization of miRNAs in these fields is anticipated to contribute to rapid testing.(Inal et al. 2013; Mitchell et al. 2008; Montani et al. 2015) Rapid and simple detection methods are needed to permit the application of these miRNA detection tests in the environmental and biomedical fields as fast screening tools.(Fiammengo 2017; Graybill and Bailey 2016)

In past decades, numerous oligonucleotide detection techniques have been developed aiming at fast, rapid, and simple screening based on electrochemical, gravimetric and optical

techniques.(Sassolas et al. 2008) Surface plasmon resonance (SPR) imaging is an optical technique that enables real-time and multiplexed detection of biomolecules on an SPR chip in a parallel manner without labeling the target biomolecules (label-free) or without any contact or wiring normally used in electrochemical techniques.(Smith and Corn 2003; Spoto and Minunni 2012) SPR imaging-based biomolecular sensing is based on the changes in SPR images before and after molecular recognition, yielded by subtraction of pre-recognition images from post-recognition images of the SPR sensors on an SPR chip to provide molecular recognition. The more target biomolecules are bound to the sensors, the higher the contrast is obtained by the sensors.

Previously, we developed a miRNA detection method based on SPR imaging with signal amplification that employed polyadenine (poly(A)) extension at the miRNA terminal and Au nanoparticles (AuNPs) binding to the poly(A) tails after hybridization of the miRNA to the complementary locked nucleic acid (LNA) probe.(Fang et al. 2006) This method achieved detection at the 10-fM level using a combination of AuNPs and polymerases. AuNPs were also used for attomole detection of mesophilic DNA polymerase products,(Gifford et al. 2010) and for measuring the binding of proteins to single-stranded DNA aptamers based on DNAzyme hydrolysis of the aptamers.(Chen and Corn 2013) Many other groups have reported metal nanoparticles-based SPR detection as well, because the nanoparticles, especially AuNPs, have remarkable SPR properties as enhancers of SPR electromagnetic field, helping signal amplification and high sensitive detection.(Coutinho and Somoza 2019; Zeng et al. 2014) The multiple signal amplification strategy based on the combination of AuNPs and AgNPs detected of miRNAs with the detection limit of 0.6 fM.(Liu et al. 2017) The competitive hybridization of target miRNAs with AuNP-DNAs showed the detection limit of 500 pM for the targets.(Hong et al. 2018) Metal nanoparticles were also used for single-molecule investigation of thermodynamics of miRNAs based on local SPR (LSPR).(Chen et al. 2018)

For simplicity and rapidity of miRNA detection, in this study, we have developed a SPR signal amplification method based on miRNA-detection-selective precipitation of organic

compounds, instead of metal nanoparticles, to demonstrate sequence-specific and simultaneous miRNA detection at the attomole level. MiRNAs as lung cancer RNA biomarkers were detected on a single SPR chip possessing the probe DNA-modified sensors, incubated in solutions containing different target miRNA concentrations. Selective signal amplification of the miRNA detection was achieved by utilizing the combination of hybridization of the miRNA to a complementary probe DNA, followed by extension of poly(A) tails of the miRNA by poly(A) polymerase, selective binding of horseradish peroxidase (HRP) to the poly(A) tails, and H_2O_2-mediated oxidation of tetramethylbenzidine (TMB) catalyzed by the HRP and resultant precipitation of oxidized TMB (Ox-TMB).(Bos et al. 1981; Josephy et al. 1982) The target miRNAs were sequence-specifically and simultaneously detected at the pM level, equivalent to amol-level in 1 μL of miRNA solution on 16 oligonucleotide sensors fabricated on a single SPR chip. TMB-based signal enhancement is popularly used in biochemical staining processes, including immunohistochemistry enzyme-linked immunosorbent assays (ELISA) as a visualizing reagent.(Frey et al. 2000; Rhee et al. 2010) Besides these calorimetric techniques, TMB is also widely used in electrochemical techniques,(Akter et al. 2017; Fanjul-Bolado et al. 2005; Labib et al. 2016; Shen et al. 2014) QCM,(Alfonta et al. 2000; Chen et al. 2015) and SPR(Li et al. 2007; Linman et al. 2010; Phillips et al. 2007) for signal enhancement. We believe this to be a simple, cost-effective, and feasible signal amplification method based on an organic compound, TMB, rather than metal nanoparticles.

2. Experimental

2.1 Reagents

The sequences used in this study were from the National Center for Biotechnology Information (NCBI). Oligo-DNAs and RNAs were purchased from Integrated DNA Technologies (Skokie, IL) or Europhins Genomics (Tokyo, Japan), with the sequences of 5'-ATT TGA CAA ACT GAC A-NH_2-3' (from hsa-miR-223, DNA-NH_2_miR223), 5'-TCA GTC TGA TAA GCT A-NH_2-3' (from hsa-miR-21, DNA-NH_2_miR21), 5'-GTG CCT TCA CTG CAG T-NH_2-3' (from hsa-miR-17, DNA-NH_2_miR17), 5'-AAA AAA AAA AAA AAA AAA AAA AAA AAA AAA AAA-NH_2-3' (A_{30}-NH_2), 5'-biotin-TTT TTT TTT TTT TTT TTT TTT TTT TTT TTT TTT-3' (T_{30}-biotin), 5'-UGU CAG UUU GUC AAA UAC CCC A-3' (RNA_miR223), 5'-UAG CUU AUC AGA CUG AUG UUG A-3' (RNA_miR21), and 5'-ACU GCA GUG AAG GCA CUU GUA G-3' (RNA_miR17). 11-Mercapto-1-undecane amine (MUAM) was from Dojindo (Kumamoto, Japan). Poly-glutamate sodium (p-Glu), 1-ethyl-3-(3-dimethylaminopropyl)-carbodiimide hydrochloride (EDC), and *N*-hydroxysulfosuccinimide (sNHS) were from Thermo Fisher Scientific (Waltham, MA) or Sigma-Aldrich (St. Louis, MO). Poly(A) polymerase, Proteinase K, biotinylated horseradish peroxidase (HRP-biotin), and streptavidin were from New England Biolabs (Ipswich, MA) or Thermo Fisher Scientific. The 3,3',5,5'-tetramethylbenzidine (TMB) solution was from BioFX (Owings Mills, MD) or Sigma-Aldrich. mPEG-NH_2 (MW = 1,000) was from LaysanBio (Arab, AL). SDS and H_2O_2 were from Sigma-Aldrich. A phosphate-buffered saline (PBS) was prepared from a 10-fold dilution of 10X PBS (100 mM phosphate, pH 7.4, not containing Ca^{2+} or Mg^{2+}; Fisher or Fujifilm-Wako). All aqueous solutions were prepared with deionized and charcoal-treated water (specified resistance >18.2 MΩ cm), obtained using a Milli-Q reagent grade water system (Millipore; Bedford, MA).

2.2 Preparation of SPRI chips

SPRI chips (16 spots; array interval, 1.7 mm; diameter, 0.8 mm) were fabricated in a manner similar to that reported in previous papers(Fang et al. 2006) or purchased from GWC

Technologies (Madison, WI). Briefly, a mechanically polished SF-10 glass (Schott Glass; Mainz, Germany) or equivalent (e.g., S-TIH10 from Ohara, Kanagawa, Japan) was cleaned by O_2 plasma emitted from a plasma cleaner. The glass was treated with a Sigmacoat siliconizing reagent (Sigma-Aldrich) for 1 min, rinsed with hexane, ethanol, and water, and baked at 90 ˚C for 1 h. A 10 Å-thick Cr adhesion layer and a 450 Å-thick Au film were deposited on the glass covered with a stencil template of the SPRI chip pattern using a DV-502A metal evaporator (Denton Vacuum; Moorestown, NJ) or a CFS-4EP-LL sputter setup (Shibaura Mechatronics, Kanagawa, Japan). The Au surfaces were soaked in a 1 mM MUAM ethanoic solution overnight, 2 mg/mL p-Glu in PBS for 1 h, and a PBS solution containing 75 mM EDC + 15 mM sNHS + 0.25 mM DNA-NH_2 or mPEG-NH_2 overnight, as briefly described in Figure 1A. The modification layout of DNA-NH_2 and mPEG-NH_2 are depicted in Figure 1B.

2.3 miRNA detection

The detection process of the target miRNAs is briefly described in Figure 2A. One-μL aliquots of an RNA solution in PBS were dropped onto the prepared DNA-modified surface overnight (a). After RNA hybridization, the surface of the chip was covered with a flow cell with a volume of 100 μL, and a flow cell/SPRI chip/prism assembly was composed. The solutions were passed through the flow cell at a flow rate of 1 mL/min. Next, the surface was reacted with a mixture of 3 U/μL M poly(A) polymerase and 1 mM ATP in a reaction buffer containing 20 mM Tris-HCl (pH 7.0), 0.6 mM $MnCl_2$, 0.02 mM EDTA, 0.2 mM DTT, 100 μg/mL acetylated BSA, and 10% glycerol for 30 min and washed with PBS for 30 min. The condition of the enzymatic reaction was determined taking into account of that in the previous paper.(Fang et al. 2006) After the reaction, the surface was washed with 0.1 mg/mL proteinase K in PBS for 30 min, with 0.01% sodium dodecyl sulfate (SDS) in PBS for 30 min, and then with PBS for 30 min (b). The surface was then reacted with a mixture of 100 nM T_{30}-biotin, 300 nM HRP-biotin, and 100 nM streptavidin in PBS, as the ternary complex of T_{30}-biotin/HRP-biotin/streptavidin, for 30 min and then washed with PBS (c). The concentration of the ternary complex, 100 nM, was determined so as the extended poly(A)

should completely be reacted with the complex in use of 5 μM target miRNAs, referring to the previous study,(Fang et al. 2006) where the 10 nM of T_{30}-coated AuNPs was used for extended poly(A) tails in use of 500 nM target miRNAs. Finally, the surface was reacted with a mixture of 1,000 μL of TMB solution and 100 μL of 30% H_2O_2 overnight and washed with PBS for 40 min (d). TMB is oxidized to water-insoluble Ox-TMB (3,3',5,5'-tetramethylbenzidine diamine, Figure 2B), which appears as a blue precipitate, by reaction with H_2O_2 on HRP. SPR images were collected before and after each step to obtain a difference image by subtraction.

2.4 SPR imaging measurements

An SPR imager (GWC Technologies) was employed for all the SPRI experiments based on near-infrared excitation from an incoherent white light source. Briefly, as shown previously,(Fang et al. 2006) collimated *p*-polarized light was used to illuminate the flow cell/SPRI chip/prism assembly at a fixed incident angle near the SPR angle. The reflected light is directed through a band-pass filter centered at λ = 830 nm and collected with a CCD camera. The data was collected using V++ digital imaging system software (Digital Optics, Auckland, New Zealand) and further analyzed using ImageJ image analysis software (NIH; Bethesda, MD).

3. Results and discussion

3.1 SPR response of prepared sensors

The prepared sensor was used for SPR measurements. In Figure 3A, SPR responses collected from four kinds of SPR sensors on a chip were demonstrated, in which each SPR response is expressed as an average value of SPR responses for sensors modified with each species, in the range of steps from hybridization of the target RNA_miR21 to removal of nonspecific adsorption by proteinase K. The SPRI chip was covered with the flow cell to build the flow cell/SPRI chip/prism assembly, followed by flowing 5 μM RNA_miR21 in PBS. As a result, an SPR response was obtained only for the DNA-NH_2_miR21-modified sensors complementary to the target RNA_miR21, though a low level of noise or fluctuation of the sensors were observed (Figure 3B). After the extension reaction of poly(A) tails at the terminal of the target RNA by the flowing poly(A) polymerase solution in PBS for 120 min, the sequence-specificity of the SPR responses for the DNA-NH_2_miR21-modified sensors appeared to decline due to the non-coincidence of the other SPR responses. However, the flow of the proteinase K solution, 0.01% SDS in PBS, and PBS helped making their response coincident. The use of proteinase K limits signal variance when performing measurements by reducing/blocking a majority of nonspecific adsorption events. These results revealed that the extension reaction of poly(A) tails proceeds sequence-specifically. The difference of Δ%R between sensors for DNA-NH_2_miR21 and those for DNA-NH_2_miR17 (=ΔΔ%R) of 0.243 ± 0.116% (at 40 min, n = 4) in the hybridization (Figure 3B) was magnified to 1.66 ± 0.831% (at 250 min, n = 4) after the extension reaction of poly(A) tails (Figure 3C), where about 7-times enhancement of ΔΔ%R was observed. Here, we expressed the SPR responses as the gray values as well the Δ%R, for the easy comprehension of the results in the next sections. In Figure 3C, the gray value at 250 min for the DNA-NH_2_miR21-modified sensors (solid line) is 13.4, and those for the others are 5.5.

3.2 RNA detection by SPR imaging measurements

Next, to enhance SPR responses by the RNA-detection-selective enzymatic reaction,

the solution of the ternary complex of T_{30}-biotin/HRP-biotin/streptavidin was passed through the flow cell. Hybridization of their T_{30} with poly(A) tails was expected to make the sensors react with the target RNA obtain their HRP. In this study, we immobilized not only the DNA-NH_2_miR21 as the complementary probe, but also the DNA-NH_2_miR17 as the noncomplementary probe, A_{30}-NH_2 as the positive control, and mPEG-NH_2 as the negative control on the chip, for comparison. In this study, we use a 5 nM RNA solution instead of a 5 μM RNA solution used in the previous section, 3.1, because of the demonstration of the sensor responses for lower RNA concentrations.

The prepared SPR chip was soaked in 5 nM RNA_miR21 in PBS overnight for hybridization with probe DNA-NH_2s, followed by building the flow cell/SPRI chip/prism assembly, the extension reaction of poly(A) tails, the removal of nonspecifically adsorbed species, and the reaction with the ternary complex of T_{30}-biotin/HRP-biotin/streptavidin. Figure 4A shows an SPR image (subtraction of the SPR image collected in the hybridization of the target RNA, the same afterwards) after the reaction with the ternary complex. The SPR response for the sensor modified with DNA-NH_2_miR21 appeared larger than those for the other sensors. Comparisons using the line profiles of the image made the trend clearly observable (Figure 4B), revealing that the response for the DNA-NH_2_miR21-modified sensor was large even compared to that for the A_{30}-NH_2-modified sensor as the positive control. This shows that the reaction of the ternary complex with the poly(A) tails extended as a result of the sequence-specific hybridization of the target RNA with the probe DNA-NH_2_miR21 on the sensor. On the other hand, low SPR responses were observed in the sensors for DNA-NH_2_miR17 and mPEG-NH_2, probably due to the nonspecific adsorption of the ternary complex to the sensor surfaces. The difference in the sensor responses between the complementary probe and noncomplementary probe was about 20 as a grayscale value.

In the TMB/H_2O_2 treatment after the above reaction, TMB was oxidized to Ox-TMB on the HRP of the ternary complex to become a blue precipitate. At the same time, the SPR response of the sensor for DNA-NH_2_miR21 was markedly enlarged. In comparison, the sensors for DNA-NH_2_miR17 and mPEG-NH_2 showed quite a small increase in SPR

responses (Figure 4C). The difference in SPR responses between the DNA-NH_2_miR21 and DNA-NH_2_miR17 sensors was about 90 as a grayscale value, a 4.5-fold increase compared to before TMB/H_2O_2 treatment (Figure 4D). From these results, we concluded that TMB/H_2O_2 treatment after the reaction of the ternary complex RNA-detection selectively enhances the SPR responses.

3.3 RNA concentration dependence and limitations of the detection method

To discuss the limitations of this detection method, the same method was applied to more diluted concentrations of the target RNA. In this study, we demonstrated the sensor responses by using the other miRNA, RNA_miR17, to show the responses to the variety of RNAs. The prepared SPR chip was soaked overnight in solutions of three different concentrations: 5 nM, 50 pM, and 0.5 pM RNA_miR17 in PBS, after which the SPR signal enhancement process was applied as described in 3.2 (Figure 5A). The SPR image for the chip was subjected to the reaction with TMB/H_2O_2 as shown in Figure 5B. The line profiles of the image are shown in Figure 5C. The sensor modified with DNA-NH_2_miR17 hybridized with 5 nM RNA_miR17 showed the SPR response as a grayscale value of around 80. A similar SPR response was observed with 50 pM RNA_miR17. In contrast, the sensor showed as small a response to 0.5 pM RNA_miR17 as that to DNA-NH_2_miR21, the noncomplementary probe. Detailed study of Figure 5C showed the SPR responses for the sensors of DNA-NH_2_miR17 of 16.6±1.45, 71.7±21.1, and 65.9±13.0 for 0.5 pM, 50 pM, and 5 nM RNA_miR17, respectively, while the response for the sensor of DNA-NH_2_miR21 of 24.8±8.22 (n = numbers of pixels). The SPR response was not linear with the miRNA concentrations probably due to the multiple enzymatic signal-amplification process of the detection methodology of this study. These results reveal that the detection method is able to detect target RNAs at the picomolar level, where the amount of RNAs can be measured in attomoles when using 1 μL of miRNA solution.

Here, the sensors modified with mPEG-NH_2 as the negative control (Line 2 in Figure

5C) showed as large an SPR response as that for the sensor with DNA-NH_2_miR17 as the complementary probe. This result is different from that in Section 3.2, in that the sensor with DNA-NH_2_miR21 as the noncomplementary probe showed only a small response. From the SPR image in Figure 5B indicating an air bubble on the sensor with mPEG-NH_2, it is likely that bubbles prevented the washing-out of nonspecific absorbed Ox-TMB. Similarly, remaining Ox-TMB on the sensors with mPEG-NH_2 and DNA-NH_2_miR21 (Line 1 in Figure 5B), hindered from washing, was also observed. Air bubbles can cause unintentional false positives. This is one of the reasons why the dependence of the SPR response was not observed to be linear with the miRNA concentrations in this study. It is therefore necessary to prevent bubbles from being entrained into the flow system.

The developed method has the detection limit at the attomole level, meaning that the method needs an oligonucleotide amplification process (e.g., amplification by polymerase chain reaction (PCR)) before the detection. We believe, however, that this is a simple, cost-effective, and feasible signal amplification method based on the organic compound TMB instead of metal nanoparticles.

4. Conclusion

In this study, miRNAs as lung cancer RNA biomarkers were detected based on SPR imaging to simultaneously demonstrate selective detection and the detection limit of RNA sensors on a single SPR chip in which sensors were prepared by immobilizing probe DNAs on the Au surfaces of the chip, incubated in solutions containing different target miRNA concentrations. The target miRNAs were detected at the attomole level by simple SPR signal amplification based on the combination of sequence-specific hybridization of the target RNA to the sensors, extension reaction of poly(A) tails by poly(A) polymerase, reaction of the ternary complex of T_{30}-biotin/HRP-biotin/streptavidin, and oxidation reaction of TMB on HRP. While preserving sensitivity similar to that of methods based on metal nanoparticles, the developed miRNA detection method is a simple and cost-effective signal amplification method employing TMB as an organic molecule commonly used in biochemical staining processes, including ELISA. This is a simple, cost-effective, and feasible signal amplification method based on the organic compound TMB instead of metal nanoparticles.

This study demonstrates the limitations of this method in that the precipitated Ox-TMB resulting from oxidation of TMB was not effectively washed out in the presence of air bubbles and that the liquid flow in the flow cell accidentally flushed away the precipitated Ox-TMB. Consequently, the amplification of SPR responses might be affected by the instability of the observed Ox-TMB. More stable amplification of SPR responses is needed.

The utilization of RNA biomarkers is becoming increasingly important for the environmental and biomedical evaluations.(Alexander-Dann et al. 2018; Hayes et al. 2014; Hou et al. 2011; Mendell and Olson 2012; Wagner and Plewa 2017; Wang et al. 2016; Wang and Cui 2012) From this viewpoint, size-reduction and onsite feasibility of the biomarker detection system might be necessary.(Campana and Wlodkowic 2018; Fiammengo 2017) Some optical and electrochemical approaches for the detection system have recently been developed.(Aoki 2015; Aoki et al. 2019; Graybill and Bailey 2016) Compared to electrochemical detection systems, however, spectroscopic detection systems have in the past had a problem with miniaturization.(Sassolas et al. 2008) This was also the case with SPR.

Recently, on the other hand, newly emerged smartphone-based spectroscopic methods have been studied, and these methods are expected to assist research into the on-site detection of RNA biomarkers.(Roda et al. 2016) The method in this study, which features simple and feasible signal amplification, has potential for use in on-site detection of this type. Continuing studies on improvement of sensitivity by achieving stable signal amplification are anticipated.

Acknowledgements

This work was partially supported by JSPS KAKENHI Grant Numbers JP15K0189 and JP19K05536 (awarded to HA).

References

Akter, R., Jeong, B., Lee, Y.-M., Choi, J.-S., Rahman, M.A., 2017. Femtomolar detection of cardiac troponin I using a novel label-free and reagent-free dendrimer enhanced impedimetric immunosensor. Biosens. Bioelecton. 91, 637-643.

Alexander-Dann, B., Pruteanu, L.L., Oerton, E., Sharma, N., Berindan-Neagoe, I., Módos, D., Bender, A., 2018. Developments in toxicogenomics: understanding and predicting compound-induced toxicity from gene expression data. Mol. Omics 14(4), 218-236.

Alfonta, L., Katz, E., Willner, I., 2000. Sensing of acetylcholine by a tricomponent-enzyme layered electrode using faradaic impedance spectroscopy, cyclic voltammetry, and microgravimetric quartz crystal microbalance transduction methods. Anal. Chem. 72(5), 927-935.

Angelini, T.G., Emanueli, C., 2015. MicroRNAs as clinical biomarkers? Front. Genet. 6:240, 240.

Aoki, H., 2015. Electrochemical label-free nucleotide sensors. Chem. Asian J. 10, 2560-2573.

Aoki, H., Torimura, M., Nakazato, T., 2019. 384-Channel electrochemical sensor array chips based on hybridization-triggered switching for simultaneous oligonucleotide detection. Biosens. Bioelecton. 136, 76-83.

Bonci, D., Coppola, V., Patrizii, M., Addario, A., Cannistraci, A., Francescangeli, F., Pecci, R., Muto, G., Collura, D., Bedini, R., Zeuner, A., Valtieri, M., Sentinelli, S., Benassi, M.S., Gallucci, M., Carlini, P., Piccolo, S., De Maria, R., 2016. A microRNA code for prostate cancer metastasis. Oncogene 35(9), 1180-1192.

Bos, E.S., van der Doelen, A.A., van Rooy, N., Schuurs, A.H.W.M., 1981. 3,3′,5,5′-Tetramethylbenzidine as an ames test negative chromogen for horse-radish peroxidase in enzyme-immunoassay. J. Immunoassay Immunochem. 2(3-4), 187-204.

Campana, O., Wlodkowic, D., 2018. Ecotoxicology goes on a chip: embracing miniaturized bioanalysis in aquatic risk assessment. Environ. Sci. Technol. 52(3), 932-946.

Chen, S., Pan, D., Gan, N., Wang, D., Zhu, Y., Li, T., Cao, Y., Hu, F., Jiang, S., 2015. A QCM immunosensor to rapidly detect ractopamine using bio-polymer conjugate and magnetic β-cyclodextrins. Sens. Actuators, B 211, 523-530.

Chen, Y., Corn, R.M., 2013. DNAzyme footprinting: detecting protein−aptamer complexation on surfaces by blocking DNAzyme cleavage activity. J. Am. Chem. Soc. 135(6), 2072-2075.

Chen, Z., Peng, Y., Cao, Y., Wang, H., Zhang, J.-R., Chen, H.-Y., Zhu, J.-J., 2018. Light-driven nano-oscillators for label-free single-molecule monitoring of microRNA. Nano Lett. 18(6), 3759-3765.

Coutinho, C., Somoza, A., 2019. MicroRNA sensors based on gold nanoparticles. Anal.

Bioanal. Chem. 411(9), 1807-1824.

Fang, S., Lee, H.J., Wark, A.W., Corn, R.M., 2006. Attomole microarray detection of microRNAs by nanoparticle-amplified SPR imaging measurements of surface polyadenylation reaction. J. Am. Chem. Soc. 128, 14044-14046.

Fanjul-Bolado, P., González-García, M.B., Costa-García, A., 2005. Amperometric detection in TMB/HRP-based assays. Anal. Bioanal. Chem. 382(2), 297-302.

Fiammengo, R., 2017. Can nanotechnology improve cancer diagnosis through miRNA detection? Biomark. Med. 11(1), 69-86.

Frey, A., Meckelein, B., Externest, D., Schmidt, M.A., 2000. A stable and highly sensitive 3,3 ,5,5 -tetramethylbenzidine-based substrate reagent for enzyme-linked immunosorbent assays. J. Immunol. Methods 233(1-2), 47-56.

Fukushima, T., Hara-Yamamura, H., Urai, M., Kasuga, I., Kurisu, F., Miyoshi, T., Kimura, K., Watanabe, Y., Okabe, S., 2014. Toxicity assessment of chlorinated wastewater effluents by using transcriptome-based bioassays and Fourier transform mass spectrometry (FT-MS) analysis. Water Res. 52, 73-82.

Gifford, L.K., Sendoiu, I.E., Corn, R.M., Lupták, A., 2010. Attomole detection of mesophilic DNA polymerase products by nanoparticle-enhanced surface plasmon resonance imaging on glassified gold surfaces. J. Am. Chem. Soc. 132(27), 9265-9267.

Graybill, R.M., Bailey, R.C., 2016. Emerging biosensing approaches for microRNA analysis. Anal. Chem. 88(1), 431-450.

Hayes, J., Peruzzi, P.P., Lawler, S., 2014. MicroRNAs in cancer: biomarkers, functions and therapy. Trends Mol. Med. 20(8), 460-469.

Hofbauer, S.L., de Martino, M., Lucca, I., Haitel, A., Susani, M., Shariat, S.F., Klatte, T., 2018. A urinary microRNA (miR) signature for diagnosis of bladder cancer. Urol. Oncol. 36(12), 531.e531-531.e538.

Hong, L., Lu, M., Dinel, M.-P., Blain, P., Peng, W., Gua, H., Masson, J.-F., 2018. Hybridization conditions of oligonucleotide-capped gold nanoparticles for SPR sensing of microRNA. Biosens. Bioelecton. 109, 230-236.

Hou, L., Wang, D., Baccarelli, A., 2011. Environmental chemicals and microRNAs. Mutat. Res. Fund. Mol. Mech. Mut. 714(1-2), 105-112.

Huang, Y.C., 2013. The role of in vitro gene expression profiling in particulate matter health research. J. Toxicol. Environ. Health B 16(6), 381-394.

Huang, Y.C., Karoly, E.D., Dailey, L.A., Schmitt, M.T., Silbajoris, R., Graff, D.W., Devlin, R.B., 2011. Comparison of gene expression profiles induced by coarse, fine, and ultrafine particulate matter. J. Toxicol. Environ. Health A 74(5), 296-312.

Igarashi, Y., Nakatsu, N., Yamashita, T., Ono, A., Ohno, Y., Urushidani, T., Yamada, H., 2015.

Open TG-GATEs: a large-scale toxicogenomics database. Nucleic Acids Res. 43(Database issue), D921-D927.

Inal, J.M., Kosgodage, U., Azam, S., Stratton, D., Antwi-Baffour, S., Lange, S., 2013. Blood/plasma secretome and microvesicles. Biochim. Biophys. Acta 1834(11), 2317-2325.

Jansson, M.D., Lund, A.H., 2012. MicroRNA and cancer. Mol. Oncol. 6(6), 590-610.

Josephy, P.D., Eling, T., Mason, R.P., 1982. The horseradish peroxidase-catalyzed oxidation of 3,5,3',5'-tetramethylbenzidine. J. Biol. Chem. 257(7), 3669-3675.

Kreth, S., Hübner, M., Hinske, L.C., 2018. MicroRNAs as clinical biomarkers and therapeutic tools in perioperative medicine. Anesth. Analg. 126(2), 670-681.

Labib, M., Sargent, E.H., Kelley, S.O., 2016. Electrochemical methods for the analysis of clinically relevant biomolecules. Chem. Rev. 116(16), 9001-9090.

Leung, A.K.L., Sharp, P.A., 2010. MicroRNA functions in stress responses. Mol. Cell 40(2), 205-215.

Li, Y., Lee, H.J., Corn, R.M., 2007. Detection of protein biomarkers using RNA aptamer microarrays and enzymatically amplified surface plasmon resonance imaging. Anal. Chem. 79(3), 1082-1088.

Linman, M.J., Sugerman, K., Cheng, Q., 2010. Detection of low levels of Escherichia coli in fresh spinach by surface plasmon resonance spectroscopy with a TMB-based enzymatic signal enhancement method. Sens. Actuators, B 145(2), 613-619.

Liu, R., Wang, Q., Li, Q., Yang, X., Wang, K., Nie, W., 2017. Surface plasmon resonance biosensor for sensitive detection of microRNA and cancer cell using multiple signal amplification strategy. Biosens. Bioelecton. 87, 433-438.

Mendell, J.T., Olson, E.N., 2012. MicroRNAs in stress signaling and human disease. Cell 148(6), 1172-1187.

Mihelich, B.L., Maranville, J.C., Nolley, R., Peehl, D.M., Nonn, L., 2015. Elevated serum microRNA levels associate with absence of high-grade prostate cancer in a retrospective cohort. PLoS One 10(4), e0124245.

Min, P.K., Chan, S.Y., 2015. The biology of circulating microRNAs in cardiovascular disease. Eur J Clin Invest 45(8), 860-874.

Mitchell, P.S., Parkin, R.K., Kroh, E.M., Fritz, B.R., Wyman, S.K., Pogosova-Agadjanyan, E.L., Peterson, A., Noteboom, J., O'Briant, K.C., Allen, A., Lin, D.W., Urban, N., Drescher, C.W., Knudsen, B.S., Stirewalt, D.L., Gentleman, R., Vessella, R.L., Nelson, P.S., Martin, D.B., Tewari, M., 2008. Circulating microRNAs as stable blood-based markers for cancer detection. Proc. Natl. Acad. Sci. USA 105(30), 10513-10518.

Montani, F., Marzi, M.J., Dezi, F., Dama, E., Carletti, R.M., Bonizzi, G., Bertolotti, R.,

Bellomi, M., Rampinelli, C., Maisonneuve, P., Spaggiari, L., Veronesi, G., Nicassio, F., Di Fiore, P.P., Bianchi, F., 2015. miR-test: a blood test for lung cancer early detection. J. Natl. Cancer Inst. 107(6), djv063.

Olejniczak, M., Kotowska-Zimmer, A., Krzyzosiak, W., 2018. Stress-induced changes in miRNA biogenesis and functioning. Cell. Mol. Life Sci. 75(2), 177-191.

Phillips, K.S., Han, J.H., Cheng, Q., 2007. Development of a "membrane cloaking" method for amperometric enzyme immunoassay and surface plasmon resonance analysis of proteins in serum samples. Anal. Chem. 79(3), 899-907.

Rakszewska, A., Stolper, R.J., Kolasa, A.B., Piruska, A., Huck, W.T.S., 2016. Quantitative single-cell mRNA analysis in hydrogel beads. Angew. Chem. Int. Ed. 55, 1-5.

Rhee, S.G., Chang, T.-S., Jeong, W., Kang, D., 2010. Methods for detection and measurement of hydrogen peroxide inside and outside of cells. Mol. Cells 29(6), 539-549.

Roda, A., Mirasoli, M., Michelini, E., Di Fusco, M., Zangheri, M., Cevenini, L., Roda, B., Simoni, P., 2016. Progress in chemical luminescence-based biosensors: A critical review. Biosens. Bioelecton. 76, 164-179.

Sassolas, A., Leca-Bouvier, B.D., Blum, L.J., 2008. DNA biosensors and microarrays. Chem. Rev. 108(1), 109-139.

Shen, J., Li, Y., Gu, H., Xia, F., Zuo, X., 2014. Recent development of sandwich assay based on the nanobiotechnologies for proteins, nucleic acids, small molecules, and ions. Chem. Rev. 114(15), 7631-7677.

Siomi, H., Siomi, M.C., 2010. Posttranscriptional regulation of microRNA biogenesis in animals. Mol. Cell 38(3), 323-332.

Smith, E.A., Corn, R.M., 2003. Surface plasmon resonance imaging as a tool to monitor biomolecular interactions in an array based format. Appl. Spectrosc. 57(11), 320a-332a.

Spoto, G., Minunni, M., 2012. Surface plasmon resonance imaging: what next? J. Phys. Chem. Lett. 3(18), 2682-2691.

Wagner, E.D., Plewa, M.J., 2017. CHO cell cytotoxicity and genotoxicity analyses of disinfection by-products: An updated review. J. Environ. Sci. 58, 64-76.

Wang, J., Chen, J., Sen, S., 2016. MicroRNA as biomarkers and diagnostics. J. Cell. Physiol. 231(1), 25-30.

Wang, J., Cui, Q., 2012. Specific roles of microRNAs in their interactions with environmental factors. J. Nucleic Acids 2012, 978384.

Zeng, S., Baillargeat, D., Ho, H.-P., Yong, K.-T., 2014. Nanomaterials enhanced surface plasmon resonance for biological and chemical sensing applications. Chem. Soc. Rev. 43(10), 3426-3452.

Figure captions

Figure 1. Modification of Au spot surface deposited on the glass substrate. The surface was modified with 8-mercaptoundecane amine (MUAM), poly-glutamate sodium (p-Glue), and 1-ethyl-3-(3-dimethylaminopropyl)-carbodiimide hydrochloride (EDC)/*N*-hydroxysulfosuccinimide (sNHS)/DNA-NH_2 or mPEG-NH_2) (A). The layout shows DNA-NH_2_miR17, DNA-NH_2_miR21, A_{30}-NH_2, and mPEG-NH_2 modified spots (B).

Figure 2. SPR signal amplification process based on enzymatic reactions (A). The probe DNA-NH_2, tethered on the Au surface, is hybridized with the target miRNA (a). Poly(A) polymerase extends poly(A) tails at the 3' terminal of the target miRNA on the surface (b). T_{30}-biotin/HRP-biotin/streptavidin ternary complex is bound to the poly(A) tails (c). TMB is oxidized with H_2O_2 on HRP to Ox-TMB as a blue precipitate (d). Oxidation reaction of TMB to Ox-TMB (B).

Figure 3. SPR sensorgrams for DNA-NH_2_miR17 (solid line), DNA-NH_2_miR21 (dotted line), A_{30}-NH_2 (chain line), and mPEG-NH_2 (dashed line) modified Au spots in the serial treatments of (a) and (b) depicted in Figure 2A. In this case, 5 μM RNA_miR21 was used in the treatment of (a) in Figure 2A (A). The sensorgrams in the range from 0–40 min and the range from 160–250 min were enlarged (B and C, respectively). The difference of Δ%R between sensors for DNA-NH_2_miR21 and those for DNA-NH_2_miR17 was showed as ΔΔ%R.

Figure 4. The SPR image measured after the treatment of (c) in Figure 2A (A) and line profiles at line 1 and 3 (B). The SPR image measured after the treatment of (d) in Figure 2A (C) and line profiles at line 1 and 3 (D). In these cases, 5 nM RNA_miR21 was used in the treatment of (a) in Figure 2A. The areas for the sensors for DNA-NH_2_miR21 were emphasized with the asterisk (*).

Figure 5. The layout of DNA-NH_2_miR17, DNA-NH_2_miR21, A_{30}-NH_2, and mPEG-NH_2 modified Au spots and that of the solutions of 5 nM, 50 pM, and 0.5 pM RNA_miR17 used in the treatment of (a) in Figure 2A (A). SPR image measured after the treatment of (d) in Figure 2A (B) and line profiles at lines 1, 2, 3, and 4 (C). The areas for the sensors for DNA-NH_2_miR17 were emphasized with the asterisk (*).

Figure(s)

Figure 1 H. Aoki et al.

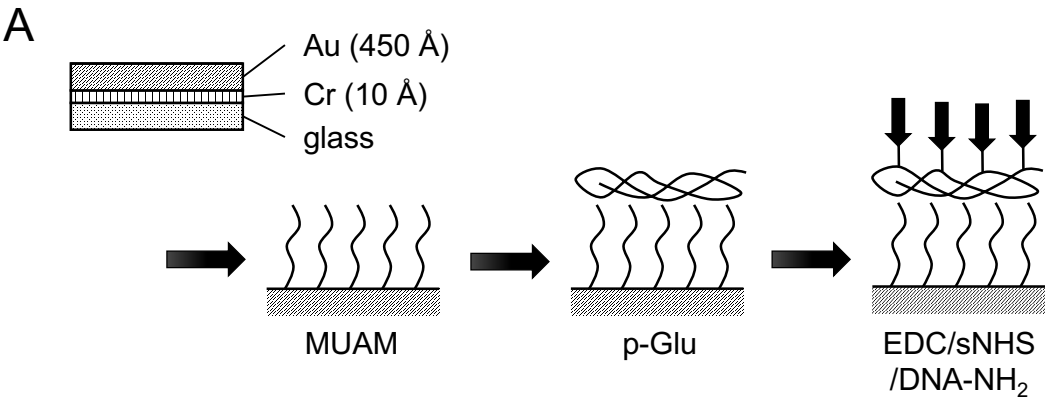

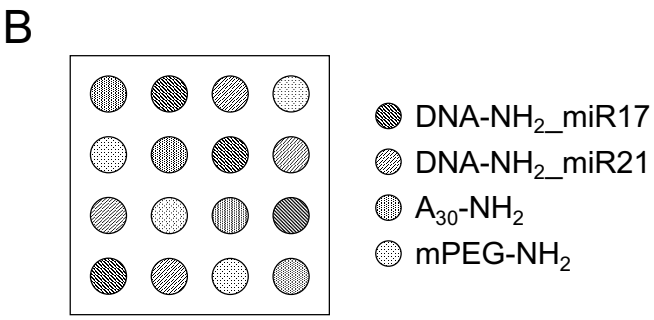

Figure 2 H. Aoki et al.

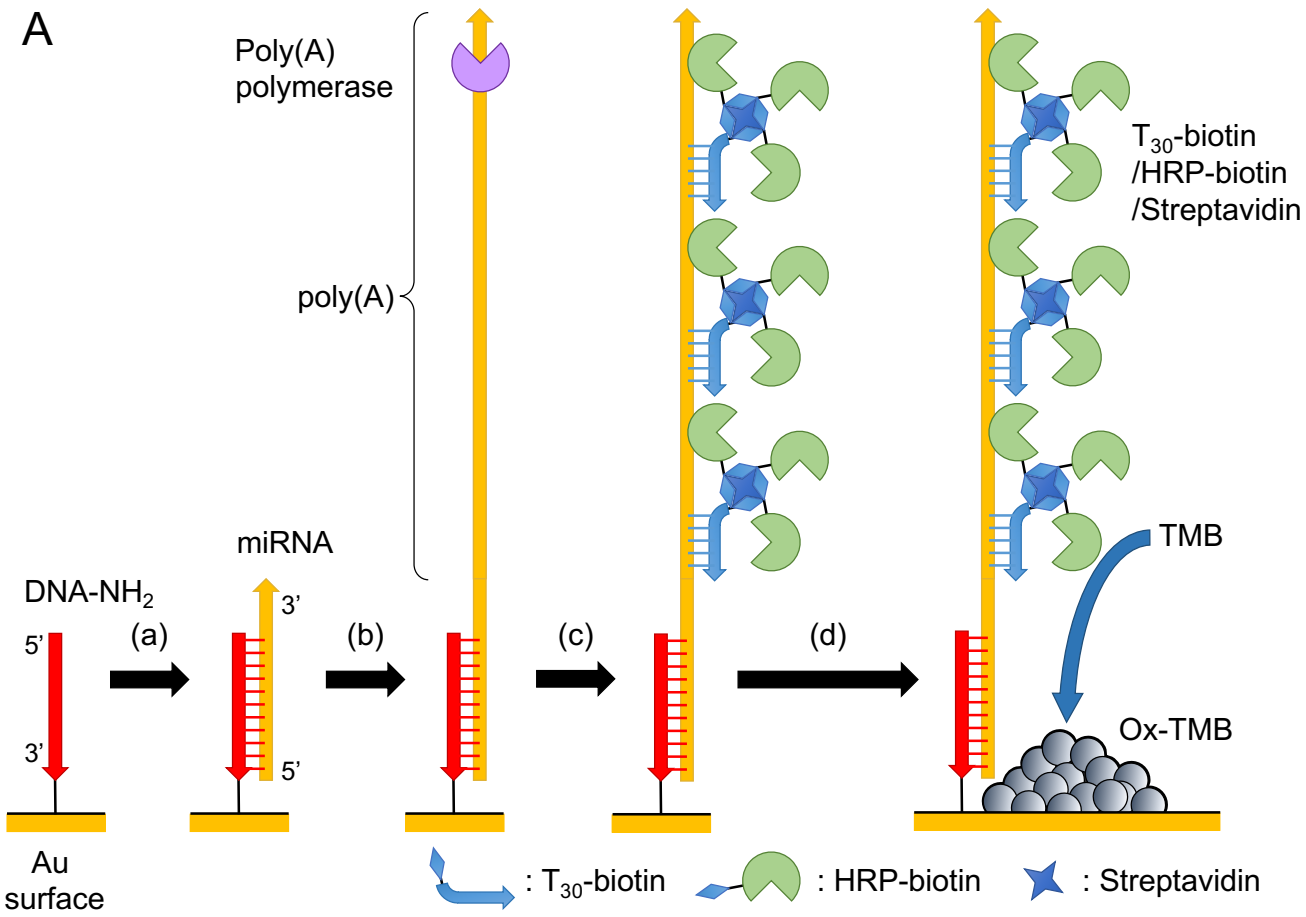

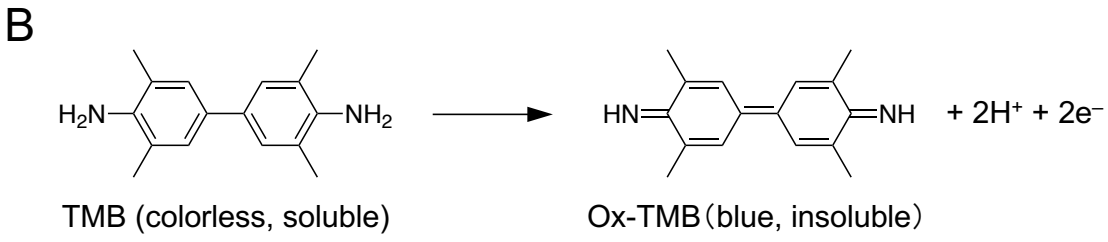

Figure 3 H. Aoki et al.

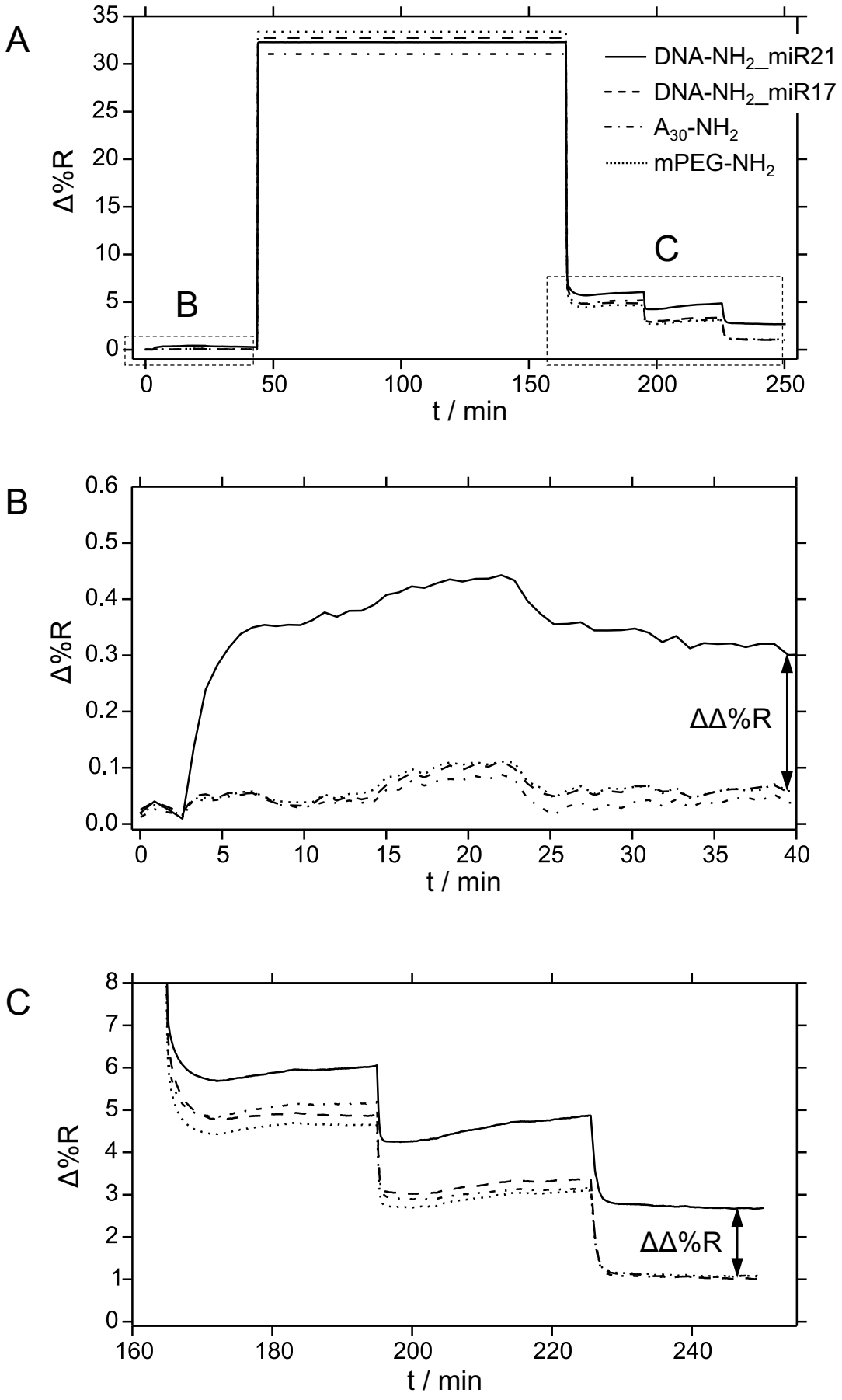

A

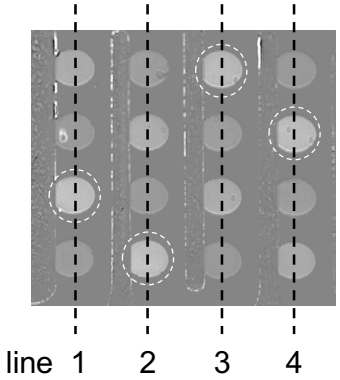
line 1
2
3
4

B

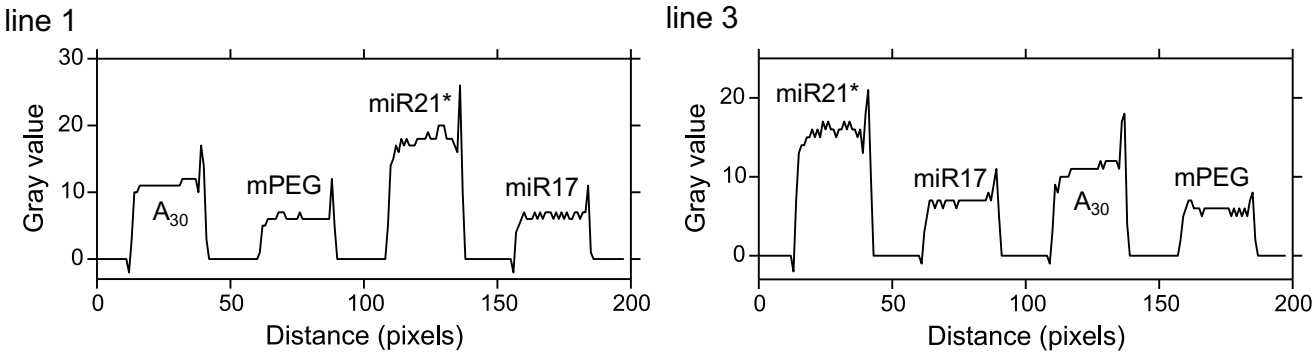
line 1
Gray value
Distance (pixels)
A30
mPEG
miR21*
miR17
line 3
Gray value
Distance (pixels)
miR21*
miR17
A30
mPEG

C

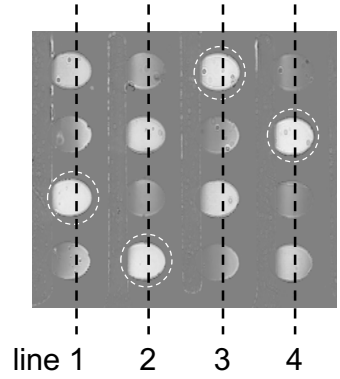
line 1
2
3
4

D

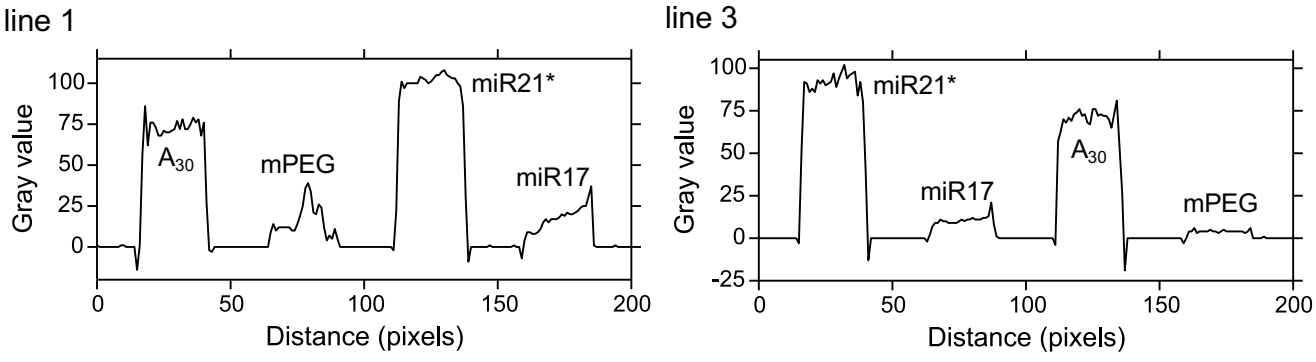
line 1
Gray value
Distance (pixels)
A30
mPEG
miR21*
miR17
line 3
Gray value
Distance (pixels)
miR21*
miR17
A30
mPEG

Figure 5 H. Aoki et al.

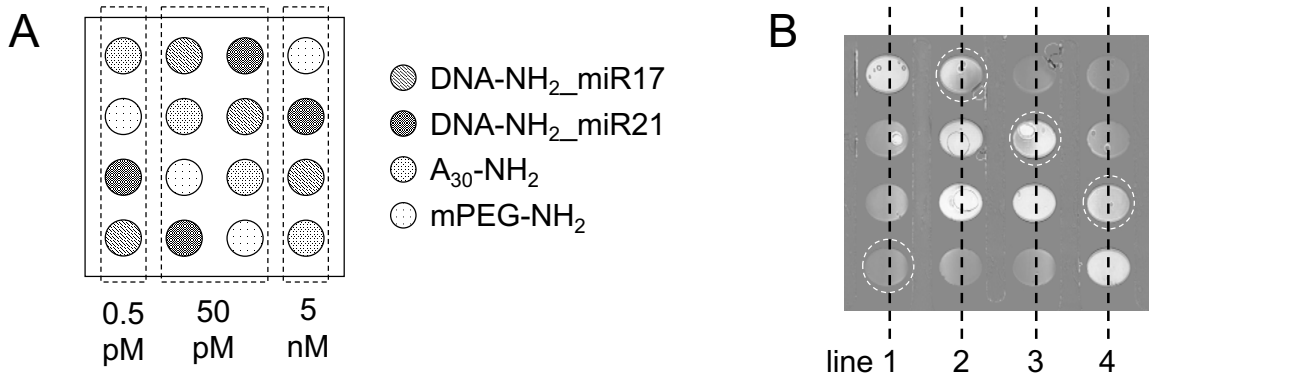

C